

Study of an Energy Storage and Recovery Concept Based on the W/WO₃ Redox Reaction: Part I. Kinetic Study and Modeling of the WO₃ Reduction Process for Energy Storage

ROMAIN HABOURY, UDAY B. PAL, PETER A. ZINK, SRIKANTH GOPALAN,
and SOUMENDRA N. BASU

Energy storage and recovery using the redox reaction of tungsten/tungsten-oxide is proposed. The system will store energy as tungsten metal by reducing the tungsten oxide with hydrogen. Thereafter, steam will be used to reoxidize the metal and recover the hydrogen. The volumetric energy density of W for storing hydrogen by this process is 21 kWh/L based on the lower heating value (LHV) of hydrogen. The main objective of this investigation was to study the kinetics of the reduction process of tungsten oxide (WO₃) and determine the optimum parameters for rapid and complete reduction. Theoretical treatment of isothermal kinetics has been extended in the current work to the reduction of tungsten oxide in powder beds. Experiments were carried out using a thermogravimetric technique under isothermal conditions at different temperatures. The reaction at 1073 K (800 °C) was found to take place in the following sequence: WO₃ → WO_{2.9} → WO_{2.72} → WO₂ → W. Expressions for the last three reaction rate constants and activation energies have been calculated based on the fact that the intermediate reactions proceed as a front moving at a certain velocity while the first reaction occurs in the entire bulk of the oxide. The gas–solid reaction kinetics were modeled mathematically in terms of the process parameters. This model of the reduction has been found to be accurate for bed heights above 1.5 mm and hydrogen partial pressures greater than 3 pct, which is ideal for implementing the energy storage concept.

DOI: 10.1007/s11663-012-9656-0

© The Minerals, Metals & Materials Society and ASM International 2012

I. INTRODUCTION

THE proposed grid-scale energy storage and recovery system is based on thermally integrating a solid-state tungsten/tungsten-oxide (W/WO₃) energy storage and recovery cycle with a reversible solid oxide electrochemical cell (RSOEC) stack. The system stores energy as tungsten metal when the RSOEC stack is operated as a steam electrolyzer using renewable and off-peak sources of electrical energy. The RSOEC electrolyzer produces hydrogen, which reduces the WO₃ to W (Figure 1) through the following reaction: WO₃(s) + 3H₂(g) → W(s) + 3H₂O(g); ΔG° = 5.7 kJ @ 1023 K (750 °C) and −5.6 kJ @ 1173 K (900 °C).^[1]

During periods of peak demand or to maintain base load conditions for renewable energy sources, the RSOEC stack is operated as a fuel cell. The hydrogen needed for the fuel cell is obtained by reducing steam

with the energy stored in the tungsten metal (Figure 1) through the following reaction: W(s) + 3H₂O(g) → WO₃(s) + 3H₂(g); ΔG° = −5.7 kJ @ 1023 K (750 °C) and 5.6 kJ @ 1173 K (900 °C).^[1]

In both the energy storage and recovery modes, steam is recycled within the system. It is clear from the preceding equations that the change in standard free energy for the storage and recovery reactions is either slightly positive or slightly negative between 1023 K and 1173 K (750 °C and 900 °C), which is the operating temperature range of RSOEC. This indicates that the equilibrium constants for the storage and the recovery reactions are near unity, which means that both of these processes will operate at near 50 pct conversion efficiency.

The current work focuses on the reduction of tungsten oxide (WO₃) with hydrogen. This publication forms the first part of the study aiming at designing and building a research scale W/WO₃ energy storage and recovery system. Studies of tungsten oxidation by water vapor and the feasibility and stability of extended and repeated cycling between the oxidation and the reduction reactions will be presented in forthcoming publications.

In the existing literature, large amounts of data are available on the hydrogen reduction of the various oxides of tungsten.^[2–10] The application of thermogravimetric methods for the determination of the activation energies of solid–gas reactions and the advantages of such methods have been discussed in several

ROMAIN HABOURY, formerly Graduate Student, École Normale Supérieure de Chimie de Paris, 7, rue Thibaud, 75014 Paris, France, is now Visiting Student, Department of Mechanical Engineering, Boston University, Boston, MA 02215. UDAY B. PAL and SOUMENDRA N. BASU, Professors, PETER A. ZINK, Research Assistant Professor and Lecturer, and SRIKANTH GOPALAN, Associate Professor, are with the Division of Materials Science and Engineering, Department of Mechanical Engineering, Boston University. Contact e-mail: upal@bu.edu

Manuscript submitted September 12, 2011.

Article published online April 7, 2012.

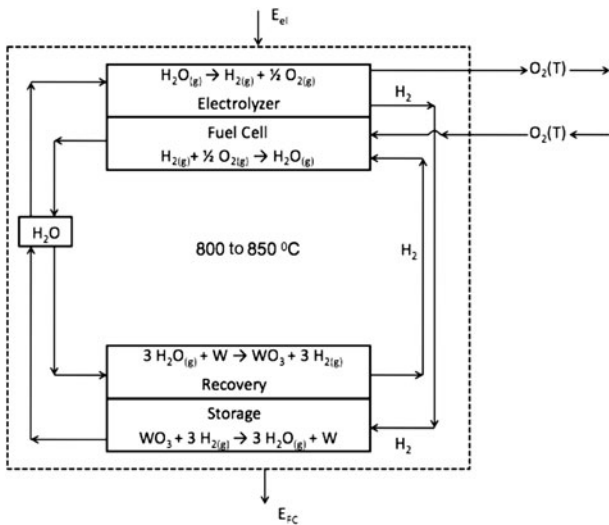


Fig. 1—Schematic of the storage and recovery concept.

publications.^[2,3] However, a lack of information seems to exist regarding the determination and the use of reaction rate constants for reaction modeling of powder beds.

The aim of this work is to apply isothermal thermogravimetric methods for the kinetic study and modeling of the reduction of tungsten oxide (WO_3) in a powder bed between 1023 K and 1173 K (750 °C and 900 °C) as a function of the bed height, hydrogen partial pressure, the particle size and bed porosity. This study helps us to understand the reduction process more completely and find the right parameters to optimize the overall reaction rate.

II. THEORETICAL CONSIDERATIONS OF SOLID-GAS REACTION

A typical reaction between a powder bed of loosely packed reactant B and gas A can be represented as follows:

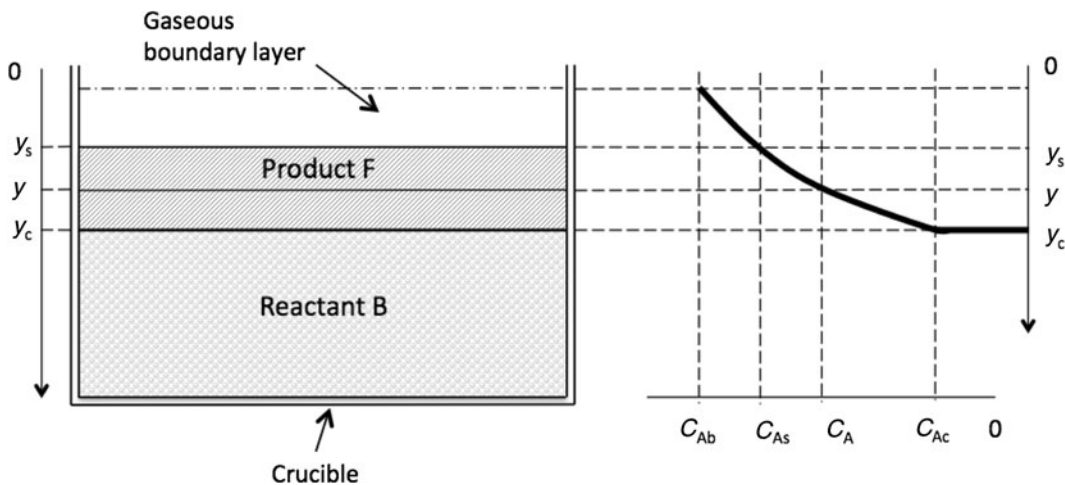
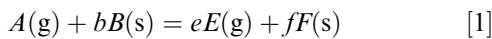


Fig. 2—Concentration profile of the gas phase in the crucible.

Consider the case where the reaction proceeds as a moving front and the temperature is uniform throughout the heterogeneous powder bed. As the reaction occurs, a layer of product F forms in place of surface particles of reactant B . The reaction product F is expected to remain porous, so A continues to diffuse through the product layer of F and react at the interface between F and the unreacted particles of B . This situation is shown in Figure 2, where the concentrations of A are labeled at various locations. The shape of the concentration profile from bulk gas to reacting front is also indicated. It is assumed that the reaction front retains its shape during the reaction, it also assumes, for convenience, that the densities of the porous product and the reactant B are the same, so that no additional gaseous region exists between the unreacted particles of B and the product layer F . One more restriction needs to be placed on the system before a simple mathematical analysis is feasible: the rate of the movement of the reaction interface at y_c , that is dy_c/dt is small compared with the diffusional flux of A through the product layer. This requirement for this pseudo-steady-state concept is valid if the density of the gas in the pores of the product layer is small compared with the density of solid reactant B . This is usually the case.

Considering pseudo-steady-state conditions, the three rates, diffusion of A through the boundary layer, diffusion through the layer of product, and reaction at the interface, are identical. The three rate equations^[11] expressed as moles of B disappearing per unit time are

$$-\frac{1}{b} \frac{dN_B}{dt} = Sk_m [C_{Ab} - C_{As}] \quad [2]$$

gas phase boundary layer diffusion

$$-\frac{1}{b} \frac{dN_B}{dt} = SD_e \left(\frac{dC_A}{dy} \right)_{y=y_c} \quad [3]$$

diffusion through product F

$$-\frac{1}{b} \frac{dN_B}{dt} = Sk C_{Ac} \quad [4]$$

reaction at the interface y_c

In these equations, b is the stoichiometric coefficient of B in Reaction [1], and S is the surface area of the exposed powder (the surface area of the powder bed).

In Eq. [2], k_m is the external mass transfer coefficient. The rate through the product layer, Eq. [3], is evaluated at $y = y_c$; D_c is the effective diffusivity of A through this porous layer. In writing Eq. [4], the chemical Reaction [1] is assumed to be first order in A and irreversible.

In the current work, the reduction process was chemical reaction controlled. Indeed, because of the fixed bed reactor, the gas phase velocity relative to that of the solid particles is high and the reaction rate was independent of the gas flow rate, therefore, the gas phase diffusion resistance is assumed to be negligible. Also for the highly porous product layer and for low conversions, diffusion resistance through the product is small, and so the reaction rate did not change with the bed thickness. Under such conditions, only the chemical step at the interface y_c (Eq. [4]) will determine the rate and the gas concentration at the interface C_{Ac} is equal to the bulk concentration C_{Ab} .

The variation of moles of B can also be expressed as

$$dN_B = \frac{dm_B}{M_B} \quad [5]$$

where dm_B is the mass variation of B and M_B is the molecular weight of B .

The concentration of gas A in Eq. [4] can be expressed as

$$C_{Ab} = \frac{P_{Ab}}{RT} \quad [6]$$

where P_{Ab} is the partial pressure of A , R is the gas constant, and T the temperature.

Combining Eqs. [4], [5], and [6] gives

$$\frac{dm_B}{dt} = -SM_B k b \frac{P_{Ab}}{RT} \quad [7]$$

The reaction rate constant k can be calculated on the basis that the velocity of the moving reaction front is constant and independent of its position in the bulk of the powder bed. If a straight line is obtained by plotting the variation of the weight over time as a function of the partial pressure of gas A , then the reaction is indeed first order and the rate constant k can be determined from the slope of the line.

Equation [7] thus provides a method to determine the reaction rate constant of a first-order solid-gas reaction at a given temperature by using different partial pressures of reactant gas A . Furthermore, the reaction rate constant k in Eq. [7] is a function of temperature and can be represented by the Arrhenius rate law:

$$k(T) = k_0 \exp\left(\frac{-Q}{RT}\right) \quad [8]$$

Substituting Eq. [8] into Eq. [7], the reaction rate can be expressed as

$$\frac{dm_B}{dt} = -SM_B k b k_0 \frac{P_{Ab}}{RT} \exp\left(\frac{-Q}{RT}\right) \quad [9]$$

$$\ln\left(\left|\frac{dm_B}{dt}\right|\right) = \ln\left(SM_B b k_0 \frac{P_{Ab}}{RT}\right) - \frac{Q}{RT} \quad [10]$$

From the slope of the plot of $\ln(dm_B/dt)$ vs $1/T$ at any given P_{Ab} , it is possible to obtain the activation energy of Reaction [1]. Equation [10] thus provides a method of using the experimental data at different temperatures to determine the activation energy of the solid-gas Reaction [1].

Reduction of tungsten oxides by hydrogen has been investigated by many studies because of its technological importance in the tungsten industry. Most authors^[4-6] agree on the stepwise reduction characteristics of WO_3 . It proceeds as $WO_3 \rightarrow WO_{2.9} \rightarrow WO_{2.72} \rightarrow WO_2$ to metallic tungsten. However, the study of Whittingham and Dickens^[7] suggested that WO_3 was reduced by hydrogen gas through $WO_{2.9}$ directly to metallic tungsten. Bustnes *et al.*^[2] observed only WO_2 as the intermediate oxide during the reduction process. The difference in the revealed reduction mechanism could be a result of the inadequate experimental resolution of reduction parameters. In the current work, the reduction kinetics of a shallow WO_3 powder bed by forming gas (Ar/H₂) were investigated by employing thermogravimetry.

III. EXPERIMENTAL DETAILS

The tungsten oxide (WO_3) powder (99.8 pct purity, 10 to 20 microns) used in this work was provided by Alfa Aesar (Ward Hill, MA). Nitrogen gas (Airgas East, Salem, NH) was used as the protective gas during the heating of the sample and during reduction as a protective gas for the electronics parts in the instrument. The forming gas (Ar/H₂ 95/5) used was supplied by Airgas East. The purge gas used was helium. Isothermal reduction studies were carried out using a SDT Q600 thermogravimetric analyzer from TA Instruments (New Castle, DE), which had a detection limit of 1 μ g. The system was controlled fully by a computer. An alumina crucible with 5.58 mm inside diameter and 3.58 mm height was employed as the container to hold the WO_3 powder bed. An alumina beam inside the furnace supported the crucible.

During heat up, a nitrogen atmosphere was maintained in the furnace using a constant nitrogen flow rate of 100 cc/min through the first carrier gas inlet connected to the balance chamber. No weight change was observed during the heat-up period. When the sample reached the reaction temperature, forming gas was introduced through the auxiliary gas inlet. In this case, the flow rate was controlled by a multigas controller from MKS Instruments, Inc. (model 647B; Andover, MA). At the end of the reaction, the forming gas flow was stopped and helium was passed through the second carrier gas inlet.

A. Effect of Temperature

The effect of the temperature on the reduction kinetics was investigated by repeating the experiments on a

0.6 mm bed height of tungsten oxide WO_3 (46 mg of powder) at 1023 K, 1073 K, 1123 K, and 1173 K (750 °C, 800 °C, 850 °C, and 900 °C).

B. Effect of Hydrogen Partial Pressure

The effect of the hydrogen partial pressure on the reduction was examined by repeating the experiments at 1073 K (800 °C) with constant nitrogen flow but different forming gas flow rates. Four forming gas flow rates were employed for the reduction (50, 67, 100, and 150 cc/min) resulting in hydrogen partial pressures of 0.0167, 0.02, 0.025, and 0.03 atm, respectively. In parallel and to examine the effect of the powder bed height on the reduction rate, five different bed heights were employed for a specific hydrogen partial pressure, namely 0.6, 0.9, 1.2, 1.5, and 1.8 mm (corresponding to 46, 69, 92, 115, and 138 mg of powder).

C. Effect of Porosity

To examine the effect of powder bed porosity, reductions with different tungsten oxide particle sizes were performed. The product from Alfa Aesar (10 to 20 μm) was heated for 4 hours at 1373 K (1100 °C) to promote particle coarsening. The resulting product, after this heat-treatment procedure, from different locations in the sample, was analyzed using X-ray diffraction (XRD) to confirm the uniformity of composition and structure. It was also verified that the composition and structure did not change as a result of the heat treatment. Then, the particles were separated using sieves of different mesh sizes. The particles sized between 75 and 106 μm with different bed heights (0.6, 0.9, 1.2, 1.5, and 1.8 mm corresponding to 43, 65, 86, 108, and 129 mg of powder, respectively) were then reduced at 1073 K (800 °C) under 0.025 atm. These results are then compared with those obtained with particles in the range of 10 to 20 μm .

During all the experiments, a computer registered the weight changes of the powder beds at intervals of 1 second; the results were then processed using Universal Analysis 2000 software (TA Instruments, Inc.). It is to be noted that all of these experiments showed excellent reproducibility.

IV. RESULTS

A. Effect of Temperature

Figures 3 and 4 present the results obtained after reducing a 0.6 mm bed height of 10 to 20 μm WO_3 particles under 0.025 atm of hydrogen. The mass change $W(\text{pct})$ represents the ratio of the actual mass to the initial mass. Considering the fact that the same mass of powder has been used for each curve, the slopes of the curves indicate that the reduction is extremely slow under the conditions used for the experiments, but the reaction rate does increase with increasing temperature.

A discontinuity in the slope is observed at approximately 99.3 pct in each reduction curve. This corresponds to the complete reduction of WO_3 to $\text{WO}_{2.9}$

(weight loss of 0.69 pct). A second discontinuity in slope is observed clearly at approximately 98.1 pct in reduction curves at 1173 K and 1123 K (900 °C and 850 °C), which is hardly noticeable for 1073 K (800 °C) and is nonexistent at 1023 K (750 °C). This discontinuity corresponds to the complete reduction of $\text{WO}_{2.9}$ to $\text{WO}_{2.72}$ (weight loss of 1.93 pct). The difficulty in noticing this transition at 1073 K (800 °C) is because of the small bed height. Additional experiments with taller bed heights show that at 1073 K (800 °C) this transition is identifiable. No such discontinuity is observed in the reduction curve at 1023 K (750 °C). The continuity in the slope of this curve would imply that at relatively low temperatures, the reduction of $\text{WO}_{2.9}$ has already taken place to some extent before the reduction of WO_3 to $\text{WO}_{2.9}$ is complete. Hence, the completion of the reduction of $\text{WO}_{2.9}$ to $\text{WO}_{2.72}$ is missing in the curve. Another discontinuity in slope is observed at approximately 93.1 pct for every reduction curve. This result corresponds to the complete reduction of $\text{WO}_{2.72}$ to WO_2 over 1073 K (800 °C) and the

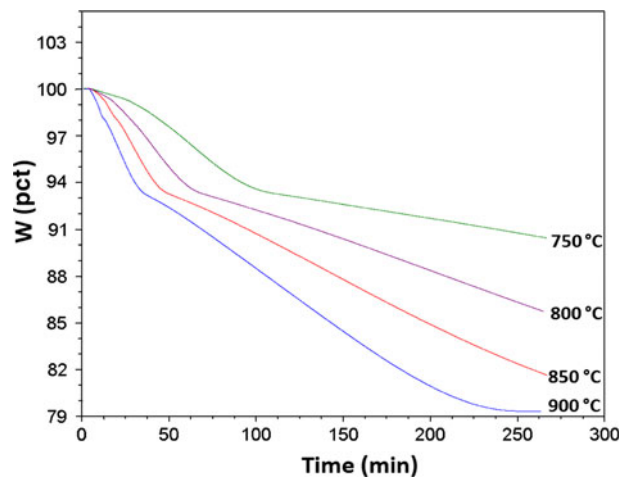


Fig. 3—Reduction curves at different temperatures under $P_{\text{H}_2} = 0.025$ atm.

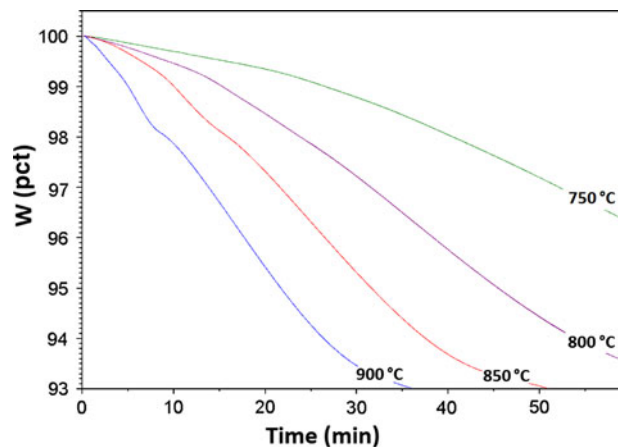


Fig. 4—Reduction curves at different temperatures (zoom) under $P_{\text{H}_2} = 0.025$ atm.

complete reduction of $\text{WO}_{2.9}$ to WO_2 under 1073 K (800 °C) (weight loss of 6.9 pct). The last discontinuity corresponds to the complete reduction of WO_2 to metallic tungsten (weight loss of 20.7 pct). No weight change is recorded after this time.

B. Effect of Hydrogen Partial Pressure

Figure 5 presents the reduction curves of a 0.9 mm bed height obtained at 1073 K (800 °C) for various hydrogen partial pressures. The reduction curves obtained under 0.025 atm of hydrogen at 1073 K (800 °C) for various bed heights with 10 to 20 μm of WO_3 particles are presented in Figure 6.

The mass change $W(\text{pct})$ represents the ratio of the actual mass to the initial mass. It is observed from Figure 5 that the reduction rate increases with increasing hydrogen partial pressure. In each reduction curve, discontinuities in slope were observed at approximately $W = 99.3$ pct, $W = 98.1$ pct, $W = 93.1$ pct, and $W = 79.3$ pct, corresponding to the complete reduction of WO_3 , $\text{WO}_{2.9}$, $\text{WO}_{2.72}$, and WO_2 , respectively. This justifies the following scheme for the reduction of tungsten oxide: $\text{WO}_3 \rightarrow \text{WO}_{2.9} \rightarrow \text{WO}_{2.72} \rightarrow \text{WO}_2 \rightarrow \text{W}$.

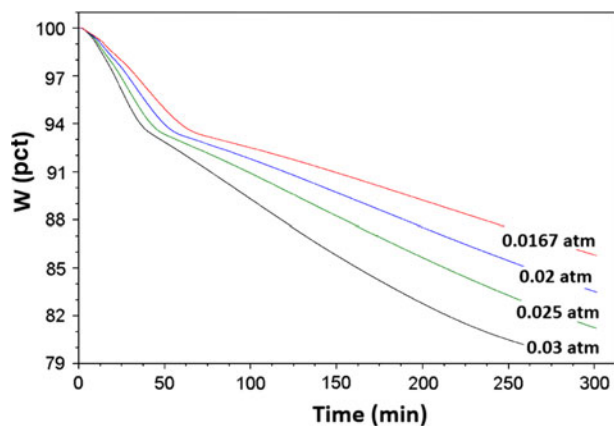


Fig. 5—Reduction curves for a 0.9-mm bed height under different P_{H_2} at 1073 K (800 °C).

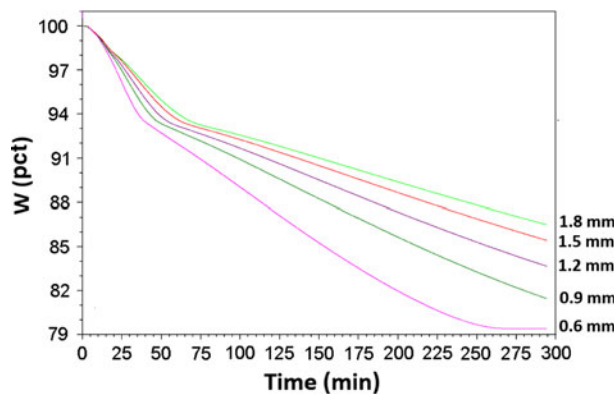


Fig. 6—Reduction curves for different bed heights at 1073 K (800 °C) and $P_{\text{H}_2} = 0.025$ atm.

Figure 6 presents the reduction curves for different bed heights under the same conditions (1073 K [800 °C] and $P_{\text{H}_2} = 0.025$ atm). It seems that for the first step ($\text{WO}_3 \rightarrow \text{WO}_{2.9}$), all the curves overlap. This means this step is a bulk reaction that depends only on the partial pressure of hydrogen. The effect of the hydrogen partial pressure on the weight loss rate for this first step ($\text{WO}_3 \rightarrow \text{WO}_{2.9}$) is presented in Figure 7.

The reduction curves obtained under 0.025 atm of hydrogen at 1073 K (800 °C) for various bed heights are presented in Figure 8. In this figure, the reaction rate is expressed by Δm , which is the weight loss in grams as a function of time. The time required for the completion of the reduction of each step ($\text{WO}_{2.9} \rightarrow \text{WO}_{2.72} \rightarrow \text{WO}_2 \rightarrow \text{W}$) is indicated by the three discontinuities in slope of each reduction curve, and the time increases with the increase of the bed height. Portions of the respective curves for each bed height for the reduction of $\text{WO}_{2.9}$ to $\text{WO}_{2.72}$, $\text{WO}_{2.72}$ to WO_2 , and WO_2 to W are parallel. The fact that $\Delta m/\Delta t$ for each step of the reduction is independent of the bed height indicates that the reaction front in the powder bed was moving at a constant velocity in each of the three stages. It is also to be noted from Figure 8 that

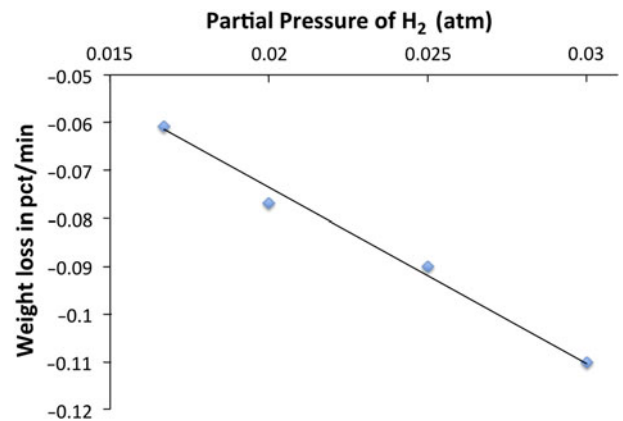


Fig. 7—Weight loss rate ($\text{WO}_3 \rightarrow \text{WO}_{2.9}$) under different P_{H_2} at 1073 K (800 °C).

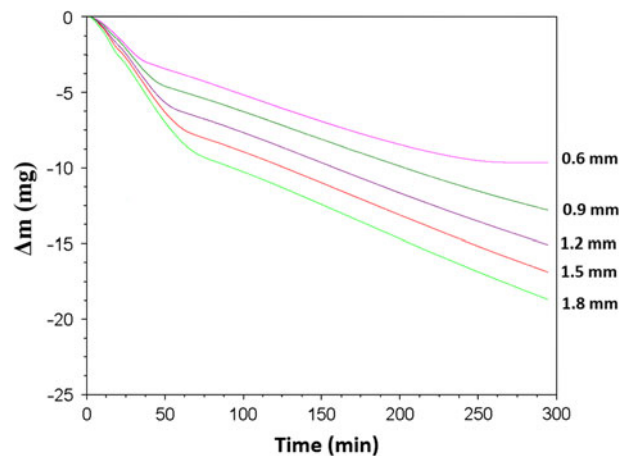


Fig. 8—Reduction curves for different bed heights at 1073 K (800 °C) under $P_{\text{H}_2} = 0.025$ atm.

$\Delta m/\Delta t$, which is a measure of the reaction front velocity, changes between the reduction stages.

It can also be observed in Figure 6 that the reaction rate curves show a little rounding near the end of each reduction step (slightly before $W = 99.3$ pct, $W = 98.1$ pct, $W = 93.1$ pct, and $W = 79.3$ pct). This result could occur because the moving reaction front is disturbed when the reaction front is too close to the bottom of the bed, which explains why the transition from $WO_{2.9}$ to $WO_{2.72}$ is hardly noticeable on low bed height reduction curves. The same trends are observed under all the different hydrogen partial pressures used.

For each reduction step ($WO_{2.9}$ to $WO_{2.72}$, $WO_{2.72}$ to WO_2 , and WO_2 to W), average values of the slopes $\Delta m/\Delta t$ per unit area of the bed are plotted as a function of the hydrogen partial pressure. These are shown in Figures 9 through 11. In consideration of the deviation of the reduction curves from linearity toward the later stages of each reduction step, data near the end of each reduction stage were not employed in the calculation of the slopes. Figures 9 through 11 also confirm that the reaction occurring in each of the reduction stages is first order (Eq. [7]).

C. Effect of Porosity

The porosity Φ of the powder bed can be expressed as:

$$\phi = \frac{V_V}{V_T} \quad [11]$$

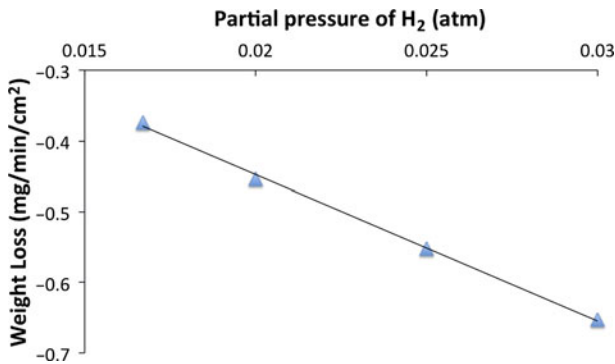


Fig. 9—Weight loss rate ($WO_{2.9} \rightarrow WO_{2.72}$) under different P_{H_2} at 1073 K (800 °C).

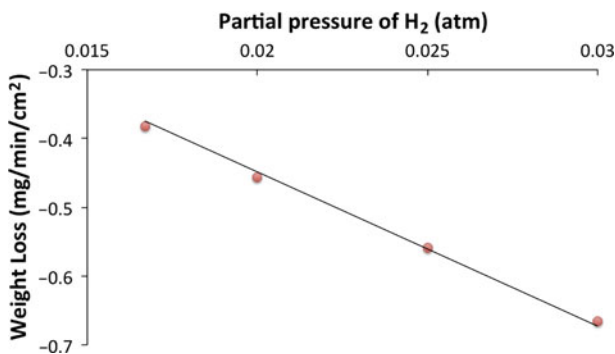


Fig. 10—Weight loss rate ($WO_{2.72} \rightarrow WO_2$) under different P_{H_2} at 1073 K (800 °C).

where V_V is the volume of void space and V_T is the total volume including the solid and the void. The volume of the void space can be calculated from the difference between the total volume and the theoretical volume V_{th} that the solid should fill. The expression for the porosity becomes

$$\phi = \frac{V_T - V_{th}}{V_T} \quad [12]$$

In the current experiments, the powder bed with tungsten oxide from Alfa Aesar (10 to 20 μm) has a porosity of 0.56. The powder bed with the coarsened particle size that was used (75 to 106 μm) has a porosity of 0.59.

The reduction curves obtained with the 75 to 106 μm powder under 0.025 atm of hydrogen at 1073 K (800 °C) for various bed heights are presented in Figure 12. The mass change W (pct) in Figure 12 once again is the ratio of the actual mass to the initial mass. The discontinuities corresponding to the formation of $WO_{2.9}$, WO_2 , and W are observed once again. However, the reduction stage $WO_{2.9} \rightarrow WO_{2.72}$ is not clearly visible. All the reduction curves are overlapped for the first step ($WO_3 \rightarrow WO_{2.9}$) indicating that the first

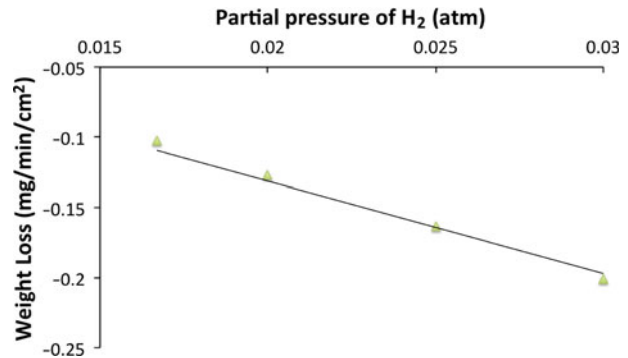


Fig. 11—Weight loss rate ($WO_2 \rightarrow W$) under different P_{H_2} at 1073 K (800 °C).

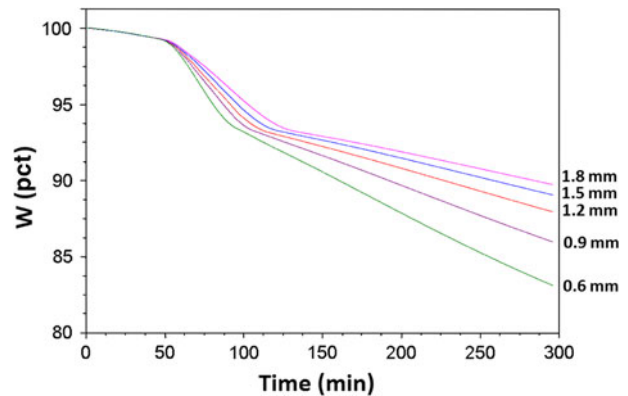


Fig. 12—Reduction curves for different bed heights at 1073 K (800 °C) and $P_{H_2} = 0.025$ atm.

reduction stage for the larger particles also occurs throughout the bulk (bulk reaction mechanism).

Figure 13 shows the previous reduction curves of the larger particles (75 to 106 μm) expressed in terms of mass loss (Δm) in grams as a function of time. The reduction behavior was found to be similar to that of the smaller particles. The time required for the completion of the reduction of each step ($\text{WO}_{2.9} \rightarrow \text{WO}_2 \rightarrow \text{W}$) increased with the increase of the bed height and the rate of reduction of each stage ($\Delta m/\Delta t$) was independent of the bed height. This finding indicates that the moving reaction front mechanism also holds for larger particles.

Figure 14 shows the reduction curves of a 1.5-mm bed height obtained at 1073 K (800 °C) under 0.025 atm of hydrogen for both particle sizes. The mass change is expressed by Δm . The linear portion on both curves corresponding to the respective formation of WO_2 and of W are parallel. The results of the other bed heights follow the same trend, which indicates that the particle size in the range measured has no effect on the velocity of the reaction front as it moves through the bed. However, the bulk reaction rate is faster for smaller particles before the moving front mechanism starts.

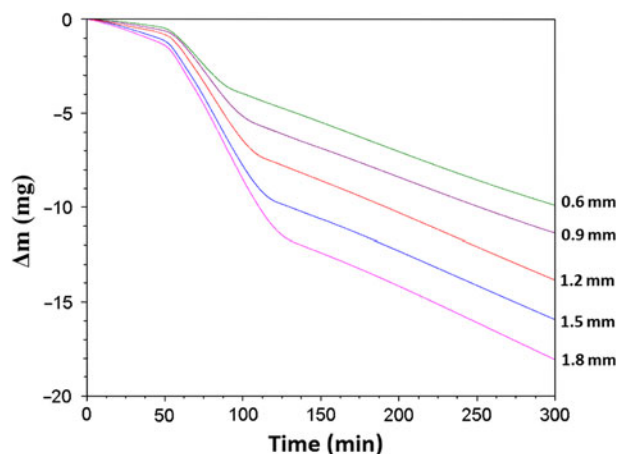


Fig. 13—Reduction curves for different bed heights at 1073 K (800 °C) and $P_{\text{H}_2} = 0.025$ atm.

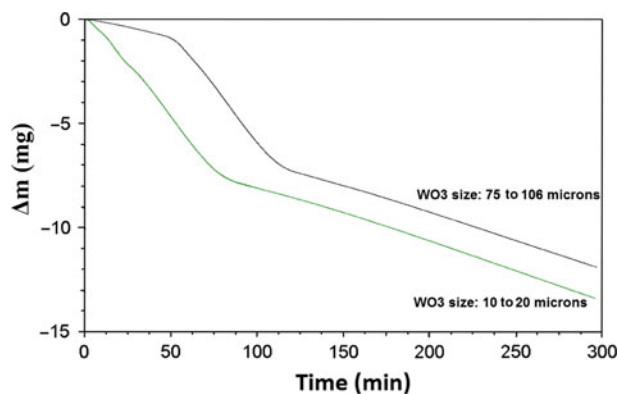
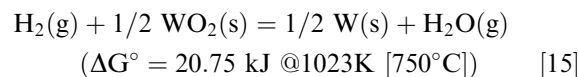
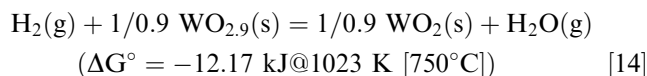
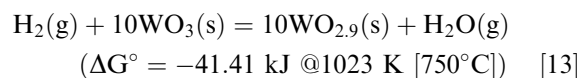


Fig. 14—Reduction curves of a 1.5-mm bed height obtained for two particles sizes.

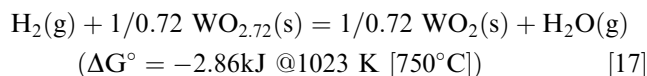
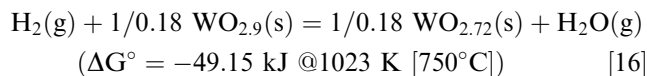
V. DISCUSSION

It is to be noted that under the current experimental conditions, it was not possible to stop the reactions at different stages of the reduction to confirm the compositions of the suboxides by XRD measurements. The thermogravimetric analysis weight loss data were used to identify the composition of the suboxides during the reduction process.

The observed discontinuities of the slope in Figure 3 would imply that at relatively low temperatures (under 1023 K [750 °C]), the reduction of WO_3 to W takes place as follows^[1]:



And imply that above 1023 K (750 °C), the reduction process involves additional steps between $\text{WO}_{2.9}$ and WO_2 ^[1]:



At 1073 K (800 °C), the weight loss rate of Reaction [13] occurs as a bulk first-order reaction, and the rate calculated from linear regression (Figure 7) is found to be 3.68 pct/min/atm. This stage in the tungsten oxide reduction process is dependent on the particle size, and the time required for the completion of this stage increases with increasing particle size.

It is observed from Figure 8 that for Reactions [15] through [17], the reaction rates are first order and are nearly constant until the end of each step, irrespective of the particle sizes and the height of the powder bed. The weight loss rate of Reaction [16] at 1073 K (800 °C) was evaluated to be 22.093 mg/min/cm²/atm from the slope of the plot in Figure 9. Similarly, the weight loss rate of Reaction [17] at 1073 K (800 °C) was found to be 22.433 mg/min/cm²/atm from the slope of the plot in Figure 10; a low thermodynamic driving force (see ΔG° s) for Reaction [17] compared with Reaction [14] is likely the reason that Reaction [16] can only be identified at higher temperatures (above 1023 K [800 °C]). Likewise, the weight loss rate of Reaction [15] at 1073 K (800 °C) was calculated to be 6.564 mg/min/cm²/atm from the slope of the plot in Figure 11.

These reactions proceed by the moving reaction front mechanism in the shallow powder bed. Because the reaction rate at a fixed partial pressure of H_2 is independent of the position of the reaction front, the transfer of H_2 to the reaction front and the removal of H_2O from there are not rate-controlling factors. Hence, it is logical to assume that Reactions [15] through [17] are all controlled by the chemical reaction occurring at the interface between the unreacted particles and the product particles in the thin layer of the reaction front.

Assuming an Arrhenius behavior, it is possible to calculate the activation energies of each of the Reactions [15] through [17] from their respective isothermal reduction rates obtained at different temperatures (shown in Figures 3 and 4). The Arrhenius plots are presented in Figures 15 through 17.

In the case of the reduction at 1023 K (750 °C), the distinct change in slope corresponding to the formation of the intermediate oxide $WO_{2.72}$ is not clear in the reduction curve shown in Figure 3. This reduction curve at 1023 K (750 °C) has not been considered for the calculation of activation energies of Reactions [16] and [17]. The activation energy of Reaction [16] was calculated to be 70.45 kJ from the slope of the Arrhenius plot in Figure 15, the activation energy of Reaction [17] was calculated to be 69.94 kJ from the slope of the Arrhenius plot in Figure 16, and the activation energy of Reaction [15] was calculated to be 84.21 kJ from the slope of the Arrhenius plot in Figure 17. The calculated

activation energy for Reaction [15] is in good agreement with the value obtained by Bustnes *et al.*^[2]

By using Eq. [7] and Figures 9 through 11, it is possible to calculate the reaction rate constants (k) of Reactions [15] through [17] at 1073 K (800 °C) as defined in Eq. [7]. These constants were calculated to be 1.52 cm/min, 6.25 cm/min, and 5.35 cm/min, respectively.

VI. MATHEMATICAL MODELING

A mathematical model was developed to predict the reduction kinetics of WO_3 . The experimental study described previously yielded the parameters necessary to model each stage of the reduction process. However, considering the intended application, the model is developed with the following assumptions:

- The reduction proceeds on a unpacked powder bed of tungsten oxide (WO_3). Hydrogen has equal access to all the surfaces of the powder bed.
- The particle size of tungsten oxide (WO_3) ranges from 10 to 20 μm .
- The system is isothermal and the temperature is fixed at 1073 K (800 °C).

In this model, the rate of each intermediate reduction step is modeled by a straight line whose slope has been calculated as described previously. An initial mass, M_0 (mg) of the tungsten oxide (WO_3) in a powder bed with a surface area of S_A (cm^2) is reduced under a partial pressure of hydrogen, P_{H_2} (atm) following the above assumptions. The reduction path is depicted in Figure 18. The mass (M_x) in Figure 18 represents the mass at the end of the reduction of the intermediate oxides. The time (t_x) represents the time necessary to transform the intermediate oxides completely.

These masses (mg) can therefore be expressed as follows:

$$M_{WO_3} = M_0 \quad [18]$$

$$M_{WO_{2.9}} = 0.9931M_0 \quad [19]$$

$$M_{WO_{2.72}} = 0.9807M_0 \quad [20]$$

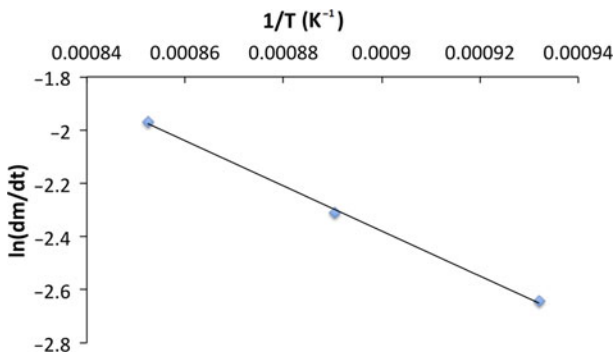


Fig. 15—Arrhenius plot for the reduction of $WO_{2.9}$ to $WO_{2.72}$.

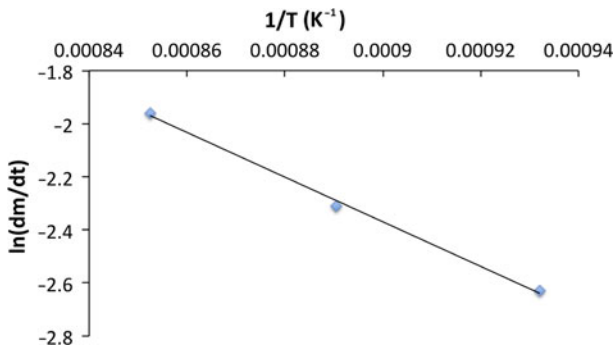


Fig. 16—Arrhenius plot for the reduction of $WO_{2.72}$ to WO_2 .

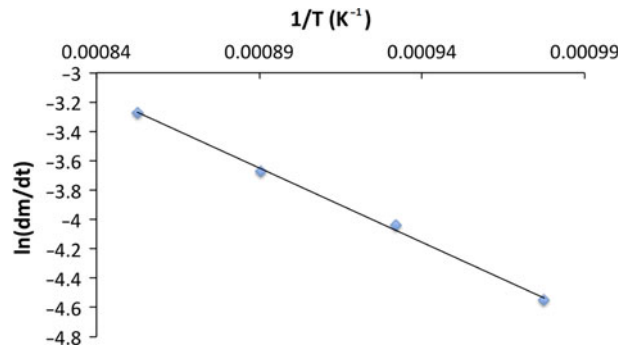


Fig. 17—Arrhenius plot for the reduction of WO_2 to W .

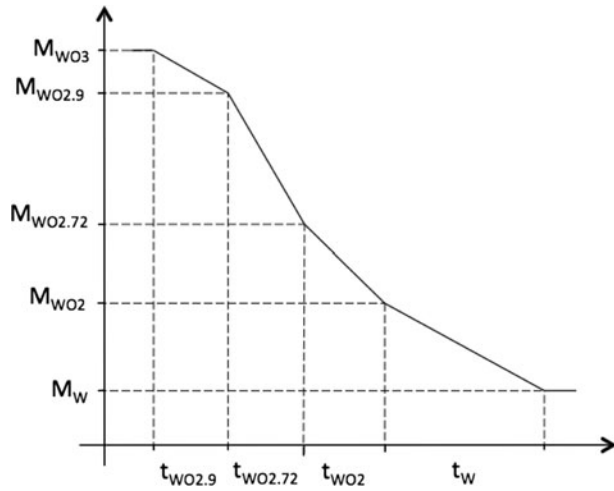


Fig. 18—Reduction scheme for modeling.

$$M_{\text{WO}_2} = 0.9310M_0 \quad [21]$$

$$M_W = 0.7930M_0 \quad [22]$$

The different times (min) can be expressed as follows:

$$t_{\text{WO}_{2.9}} = \frac{0.69}{3.68002 * P_{\text{H}_2}} \quad [23]$$

$$t_{\text{WO}_{2.72}} = \frac{M_0 * 0.0124}{22.093 * S_A * P_{\text{H}_2}} \quad [24]$$

$$t_{\text{WO}_2} = \frac{M_0 * 0.0497}{22.433 * S_A * P_{\text{H}_2}} \quad [25]$$

$$t_W = \frac{M_0 * 0.138}{6.5635 * S_A * P_{\text{H}_2}} \quad [26]$$

Time for complete reduction of the tungsten oxide (WO_3) t_{red} is

$$t_{\text{red}} = \sum_{x=\text{WO}_{2.9}}^{x=W} t_x \quad [27]$$

$$t_{\text{red}} = \frac{1}{P_{\text{H}_2}} \left[0.1875 + 0.0238 \frac{M_0}{S_A} \right] \quad [28]$$

$$t_{\text{red}} = \frac{1}{P_{\text{H}_2}} [0.1875 + 0.0238(1 - \phi)\rho H] \quad [29]$$

where ρ is the density of the tungsten oxide (mg/cm^3), Φ is the porosity of the bed as described previously, and H is the bed height (cm).

As shown in Figures 6 and 8, the mechanism, bulk or moving reaction front, is no longer strictly valid when the reaction front is close to the bottom of the bed. This finding implies that deviation of the reduction curves from linearity occurs at the end of each reduction step.

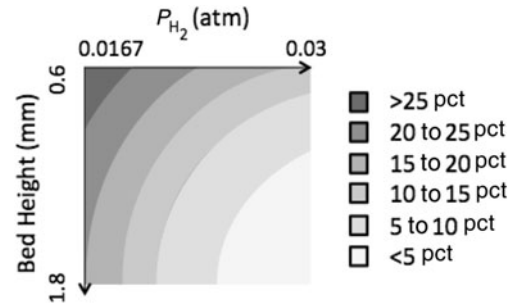


Fig. 19—Error of the experimental reduction model curves.

Therefore, for low bed height (typically lower than 1.2 mm), the linear portion of the experimental reduction curve is short, making the measurement of the slope less accurate. In other words, the average values obtained from the weight loss rates in the model will fit better for the taller beds (typically more than 1.2 mm).

As presented in Figures 7 and 9 through 11, the weight loss rates for each step increase with the increasing hydrogen partial pressure. This finding implies that the transitions between two intermediate reduction steps become much sharper with higher hydrogen partial pressure. Therefore, the deviations from the linear approximation near the bottom of the bed are less pronounced with increasing hydrogen partial pressure. Thus, this model, with linear approximation of the rates of the intermediate oxides, fits the experimental reduction curves better at higher hydrogen partial pressures.

The modeling error can be expressed as the ratio of the difference between the areas under the experimental and modeled curves to the area of the experimental curve. Figure 19 presents the evolution of this ratio as a function of the bed height and the hydrogen partial pressure. As described, the model represents a good approximation (less than 5 pct of error) of the WO_3 reduction curve when the bed height is greater than 1.5 mm and the hydrogen partial pressure is greater than 0.025 atm. The extrapolation of this model for the reduction of a 3 mm bed height of WO_3 (230 mg, 10 to 20 μm , 56 pct porosity) by pure hydrogen gives a reduction time of 23 minutes. Such a bed can be employed to design hydrogen storage system to store energy in the minutes to hours range.

VII. CONCLUSIONS

In the current work, the hydrogen reduction of tungsten oxide (WO_3) has been studied using isothermal thermogravimetry. Different temperatures, hydrogen partial pressures, particle sizes, and bed heights of tungsten oxide have been employed. The following conclusions can be drawn from this study:

1. The reduction of WO_3 to W takes place through the formation of different intermediate oxides depending on the temperature. Under 1023 K (750 °C), the reduction proceeds through the formation of $\text{WO}_{2.9}$ and WO_2 , and over 1023 K (750 °C), the reduction

proceeds through an additional intermediate tungsten oxide $WO_{2.72}$. All the reactions are first order in hydrogen concentration.

- At 1073 K (800 °C), reaction kinetics of the first stage involve a bulk reduction of WO_3 to $WO_{2.9}$, which increase with decreasing particle size. The three others stages, $WO_{2.9}$ to $WO_{2.72}$, $WO_{2.72}$ to WO_2 , and WO_2 to W, are controlled by a moving reaction front mechanism, independent of the particle size.
- The reduction rates of WO_3 and all the intermediate oxides followed Arrhenius behavior and their activation energies were determined; the error in the data increased as the bed height and the partial pressure of hydrogen decreased. The last stage of the process, the reduction of WO_2 to W, is the limiting reaction, presenting the highest activation energy (84.21 kJ/mol).
- The kinetics of the reduction at 1073 K (800 °C) were modeled as a function of the following reduction parameters: hydrogen partial pressure, the top exposed area of the powder bed, and the initial mass of WO_3 . This model is applicable for reducing WO_3 bed heights above 1.5 mm under more than 2.5 pct hydrogen. The model can be employed for designing a large-scale hydrogen storage system using WO_3 powder beds.

ACKNOWLEDGMENTS

The financial support of the Boston University (Ignition Award) is gratefully acknowledged. The assistance of Mr. Jarrod Milshtein and Dr. Stephen Topping is greatly appreciated.

REFERENCES

- HSC Thermodynamic Software: *Outokumpo Res. Oy*, 5th ed., Pori, Finland, 2003.
- J.A. Bustnes, D.U. Sichen, and S. Seetharaman: *Metall. Trans. B*, 1993, vol. 24B, pp. 475–80.
- D.U. Sichen and S. Seetharaman: *Metall. Trans. B*, 1992, vol. 23B, pp. 317–24.
- D.S. Venables and M.E. Brown: *Thermochim. Acta*, 1996, vol. 285 (2), pp. 361–82.
- X.-W. Wu: *Trans. Nonferr. Met. Soc. China*, 2009, vol. 19, pp. 785–89.
- W.D. Schubert: *Int. J. Refract. Met. H.*, 1990, vol. 9, pp. 178–91.
- M.S. Whittingham and P.G. Dickens: *7th Int. Symp. on the Reactivity of Solids*, Chapman & Hall, London, U.K., 1972, pp. 640–50.
- Yuntao Cui, J. Wang, W. Liu, and X. Wang: *J. Rare Earth*, 2010, vol. 28, special issue, pp. 202–05.
- N.E. Fouad: *J. Anal. Appl. Pyrol.*, 1997, vol. 1 (44), pp. 13–28.
- A. Lackner: *Int. J. Refract. Met. Hard Mater.*, 1996, vol. 14 (5, 6), pp. 383–91.
- J.M. Smith: *Chemical Engineering Kinetics*, 3rd ed., McGraw-Hill Book Company, New York, NY, 1981, pp. 643–47.